iScience, Volume *23*

Supplemental Information

Efficient Generation and Transcriptomic Profiling of Human iPSC-Derived Pulmonary Neuroendocrine Cells

Pooja Hor, Vasu Punj, Ben A. Calvert, Alessandra Castaldi, Alyssa J. Miller, Gianni Carraro, Barry R. Stripp, Steven L. Brody, Jason R. Spence, Justin K. Ichida, Amy L. Ryan (Firth), and Zea Borok

SUPPLEMENTAL INFORMATION

Supplemental Figure Legends

Figure S1. Directed differentiation of additional human iPSC lines into iPNECs related to Figure 1. (A) Representative immunofluorescence (IF) images of iPNECs at Day 31 of differentiation derived from two additional human iPSC lines show expression of SYP, CHGA, PGP9.5 and ENO2 (all red). Scale bars = 50 µm. (B) Orthogonal projection of Day 31 of differentiation showing SYP^+ iPNEC (red) are present on the top layer of the 3D cultures. Nuclei are counterstained with DAPI (blue). Scale bar = 200 µm.

Figure S2. Expression of key PNEC markers during *in vitro* differentiation and in adult human lung related to Figure 1. Representative IF images of (A) ENO2 (scale bar = 100 µm) and (B) SYP (in red) over 31 days of iPSC differentiation and (C) adult human bronchial lung sections stained for ENO2 (red) and KRT5 (green) (scale bar = 50 µm). Nuclei are counterstained with DAPI (blue). Relative mRNA expression of (D) GRP (E) ASCL1 (F) HEY1 and (G) HES1 over the time course of differentiation; data are normalized to Day 5 of differentiation and internal control β-actin and expressed as mean ± SEM from 3 independent experiments.

Figure S3. Notch inhibition dose response to induce optimal iPNEC differentiation related to Figure 3. Representative IF images of SYP^+ iPNECs (red) and cleaved Caspase 3 (green) at Day 31 of differentiation. (A) In the presence of DAPT (1 µM, 10 µM and 20 µM). N=3 experimental replicates. Scale bars =100 µm. (B) In the presence of DBZ (0.5 µM, 2 µM and 5 µM). N=2 experimental replicates. Scale bars = 50 µm.

Figure S4. Extended Notch inhibition increases iPNEC phenotypic complexity related to Figure 3. (A) Depiction of Sholl analysis to quantify arbors in an individual image. Quantification of number of intersections and branching density for SYP^+ (B, C), $ROBO2^+$ (D, E) and $ENO2^+$ (F, G) cells at Days 31, 60 and 91 of differentiation. N=3 experimental replicates. One-way ANOVA. *p<0.05, ** p<0.01, *** p<0.001, **** p<0.0001. Scale bars = 100 µm. Nuclei are counterstained with DAPI (blue).

Figure S5. Transcriptomic analysis of Day 91 iPNECs related to Figure 4. (A) Schematic representation of iPSCs cultured at ALI with 10 µM DAPT for 91 days that were used for single-cell RNA sequencing. (B)

Correlation of selected 1171 most variable genes among two replicates (Pearson correlation coefficient, r=0.94). (C) Flowchart describing the analytical approach taken to derive an iPNEC-associated gene list comprised of 255 genes. (D) Scatter plot showing concordance of expression of Day 91 iPNECs with respect to human fetal lung-derived primary EpCAM-negative PNECs pooled from gestational weeks 15, 18 and 21.

Figure S6. ENO2 and ROBO2 expression in Day 91 iPNECs related to Figure 3, Figure 4 and Figure 5. (A) t-SNE plot showing expression of ENO2 among single cells at Day 91 of iPSC differentiation cultures. Representative IF images showing (B) ENO2 (red) co-localization with SYP (green) and (C) ROBO2 (red) co-localization with SYP (yellow) in Day 91 iPSC differentiation cultures. Scale bars = 100 µm. Nuclei are counterstained with DAPI (blue).

Figure S7. PNEC marker gene expression in a lineage-specific manner across the trajectories related to Figure 6. (A) INSM1 (B) UCHL1 (C) NCAM1 (D) SYP (E) NEUROD1 (F) ENO2.

Figure S8. Human tracheal epithelial basal cells give rise to PNECs related to Figure 6. (A) Representative IF images indicate that human adult tracheal epithelium-derived primary (HTEC) cultures are comprised of $TP63^+$ and $KRT5^+$ basal cells. Scale bars = 200µm. (B) Representative IF images indicating SYP^+ PNECs (red) in >78 day ALI cultures from human adult tracheal epithelium-derived primary basal cells (HTEC) from 3 individual donors. Scale bars = 25 µm.

Supplemental Figures

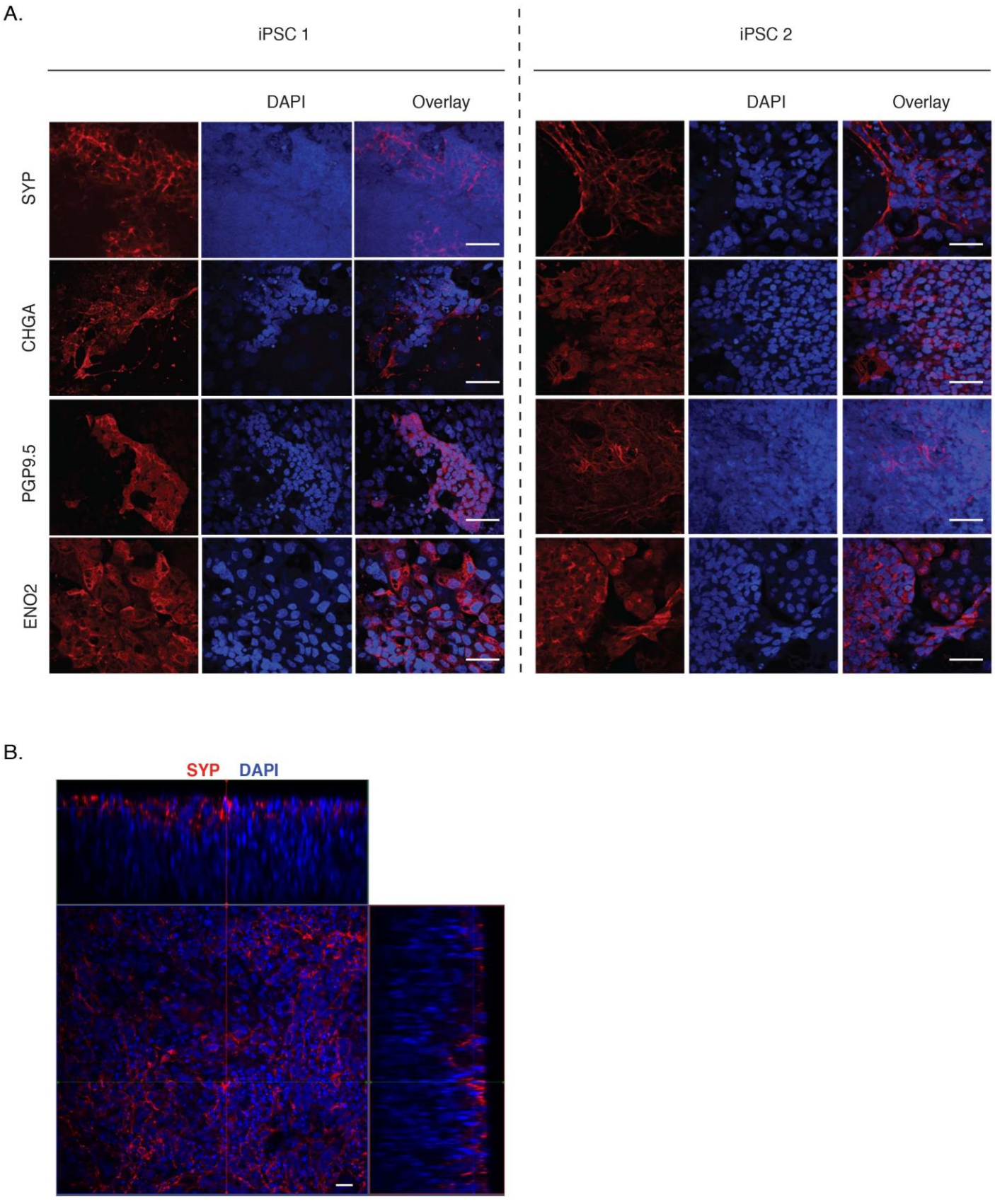

Figure S1

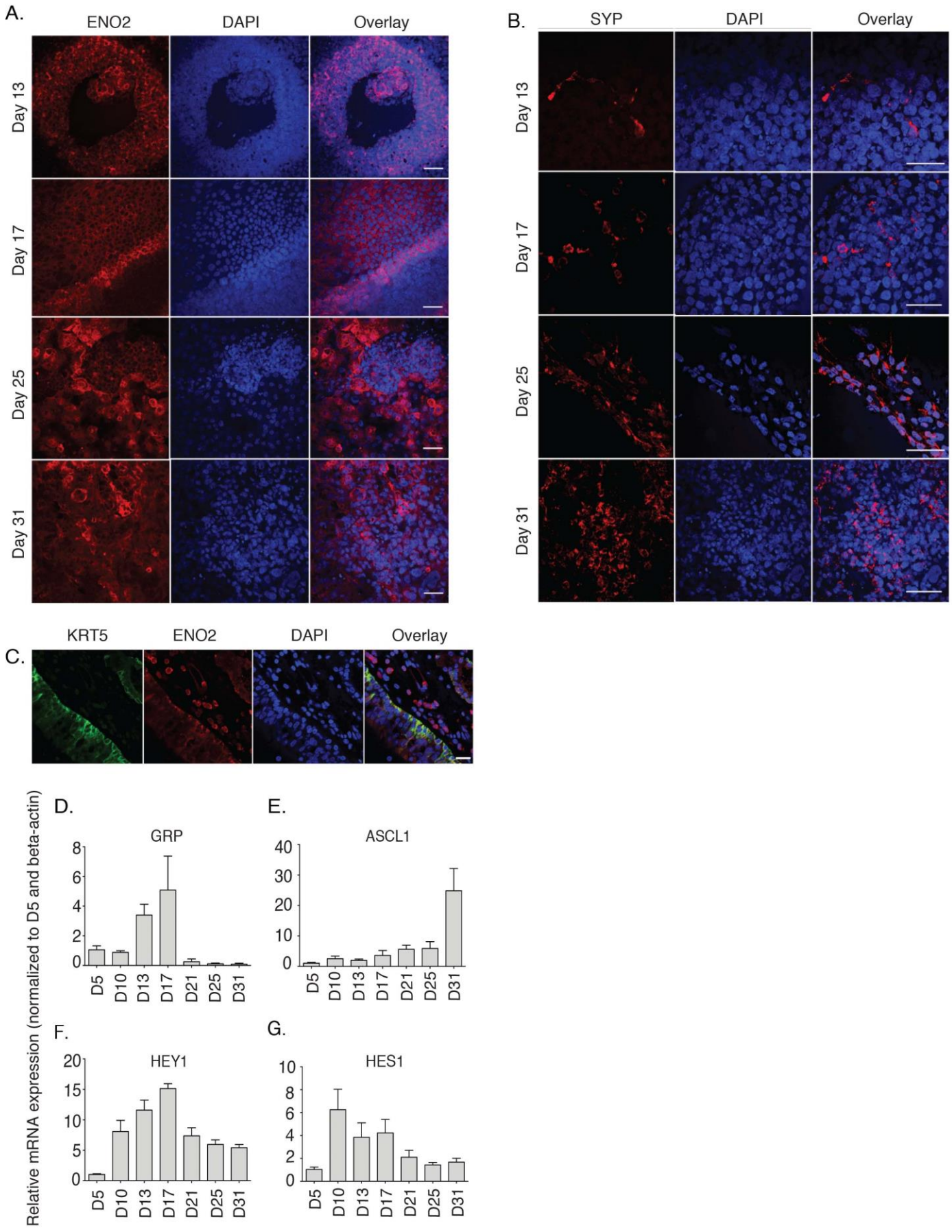
A.
ENO2
DAPI
Overlay
Day 13
Day 17
Day 25
Day 31
B.
SYP
DAPI
Overlay
Day 13
Day 17
Day 25
Day 31
C.
KRT5
ENO2
DAPI
Overlay
D.
GRP
E.
ASCL1
F.
HEY1
G.
HES1
Relative mRNA expression (normalized to D5 and beta-actin)
D5
D10
D13
D17
D21
D25
D31

Figure S2

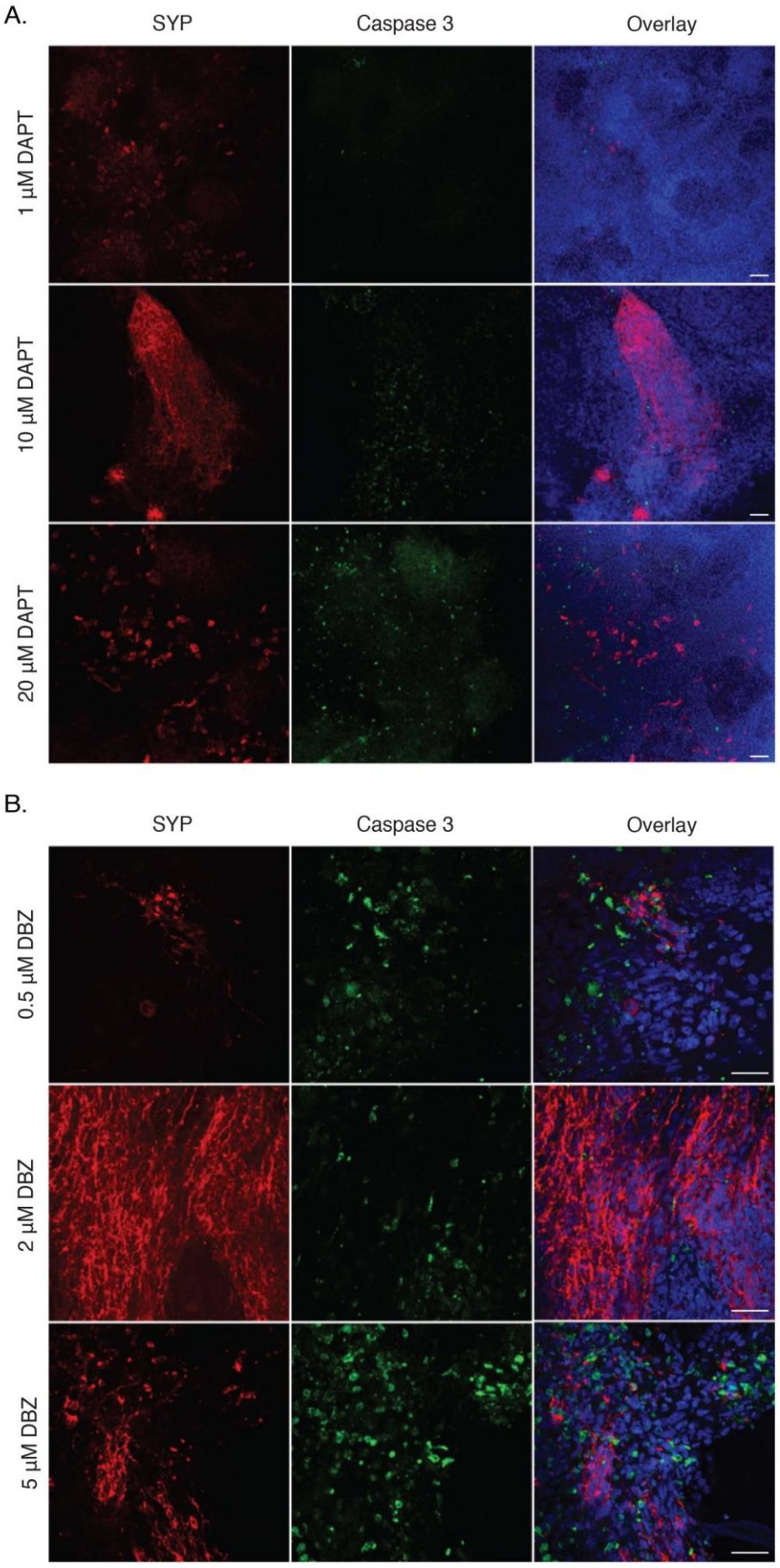
A.
SYP
Caspase 3
Overlay
1 μM DAPT
10 μM DAPT
20 μM DAPT
B.
SYP
Caspase 3
Overlay
0.5 μM DBZ
2 μM DBZ
5 μM DBZ

Figure S3

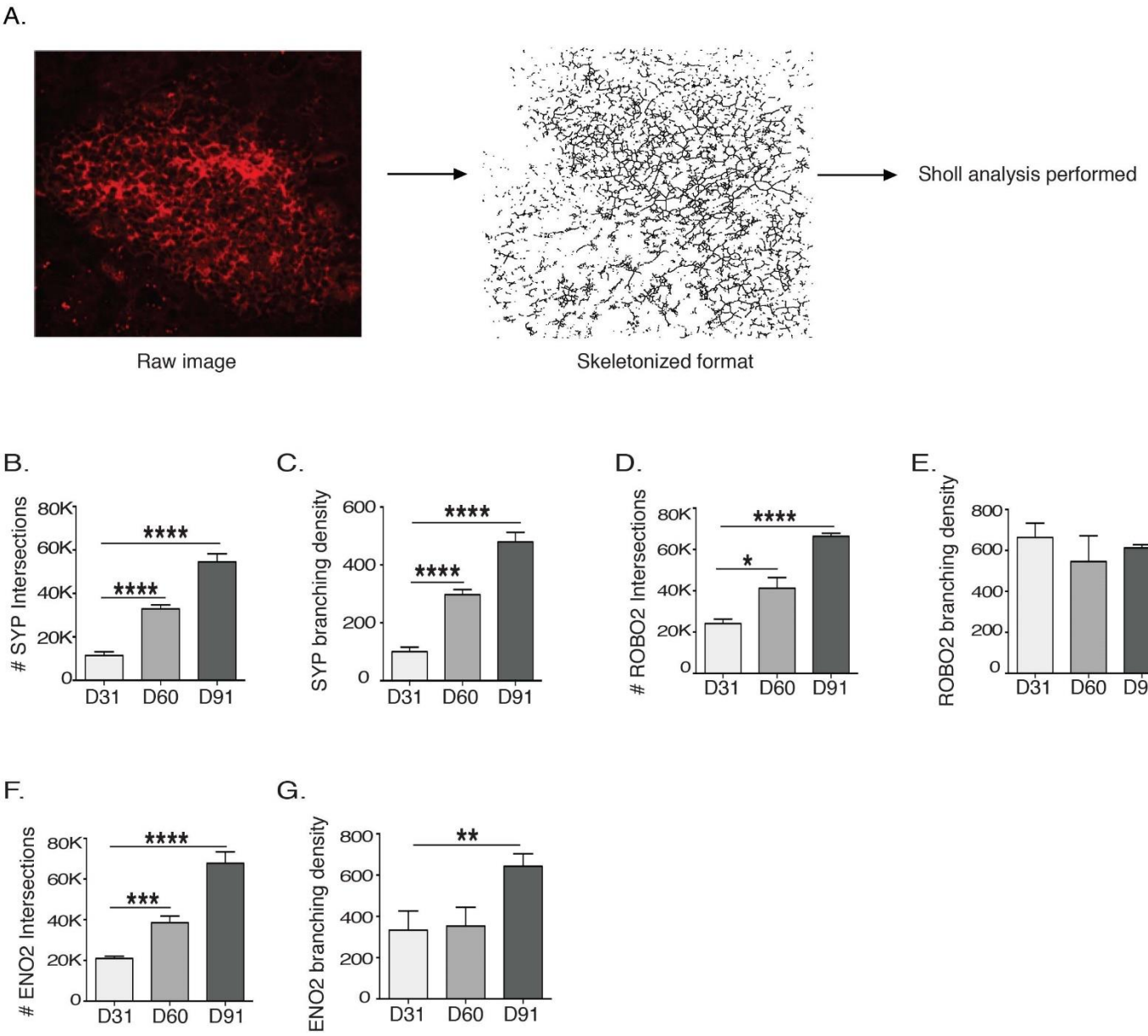
A.
Raw image
Skeletonized format
Sholl analysis performed
B.
SYP Intersections
80K
60K
40K
20K
0
****
****
D31
D60
D91
C.
SYP branching density
600
400
200
0
****
****
D31
D60
D91
D.
ROBO2 Intersections
80K
60K
40K
20K
0
****
*
D31
D60
D91
E.
ROBO2 branching density
800
600
400
200
0
D31
D60
D91
F.
ENO2 Intersections
80K
60K
40K
20K
0
****
***
D31
D60
D91
G.
ENO2 branching density
800
600
400
200
0
**
D31
D60
D91

Figure S4

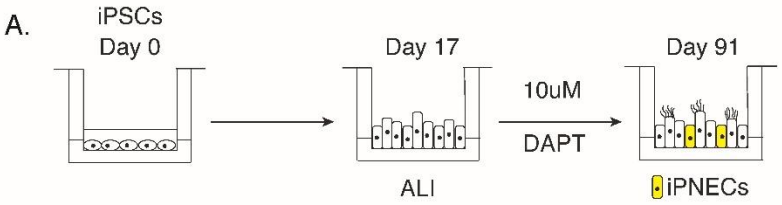
A.
iPSCs
Day 0
Day 17
ALI
10uM
DAPT
Day 91
iPNECs

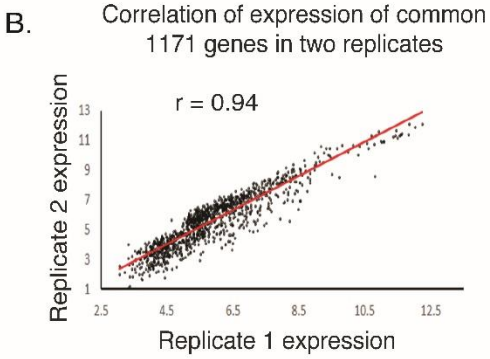
B.
Correlation of expression of common
1171 genes in two replicates
r = 0.94
Replicate 2 expression
Replicate 1 expression

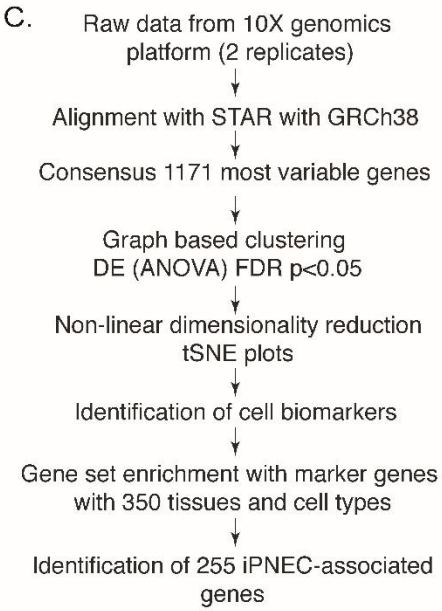
C.
Raw data from 10X genomics
platform (2 replicates)
Alignment with STAR with GRCh38
Consensus 1171 most variable genes
Graph based clustering
DE (ANOVA) FDR p<0.05
Non-linear dimensionality reduction
tSNE plots
Identification of cell biomarkers
Gene set enrichment with marker genes
with 350 tissues and cell types
Identification of 255 iPNEC-associated
genes

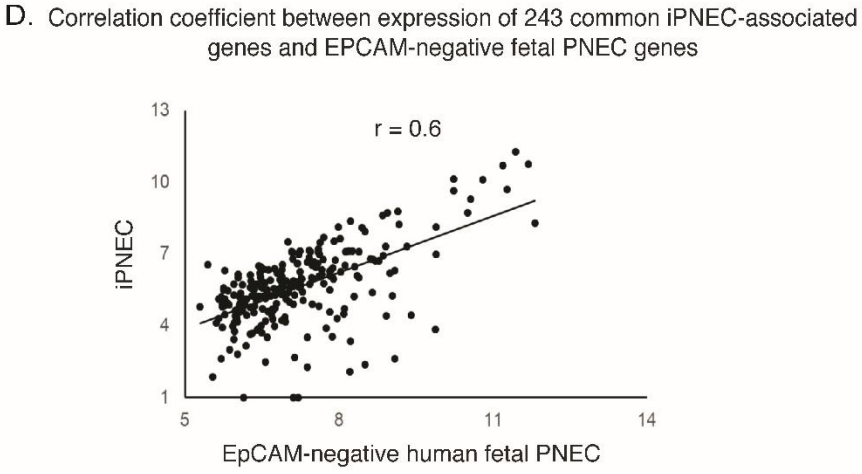
D. Correlation coefficient between expression of 243 common iPNEC-associated
genes and EPCAM-negative fetal PNEC genes
r = 0.6
iPNEC
EpCAM-negative human fetal PNEC

Figure S5

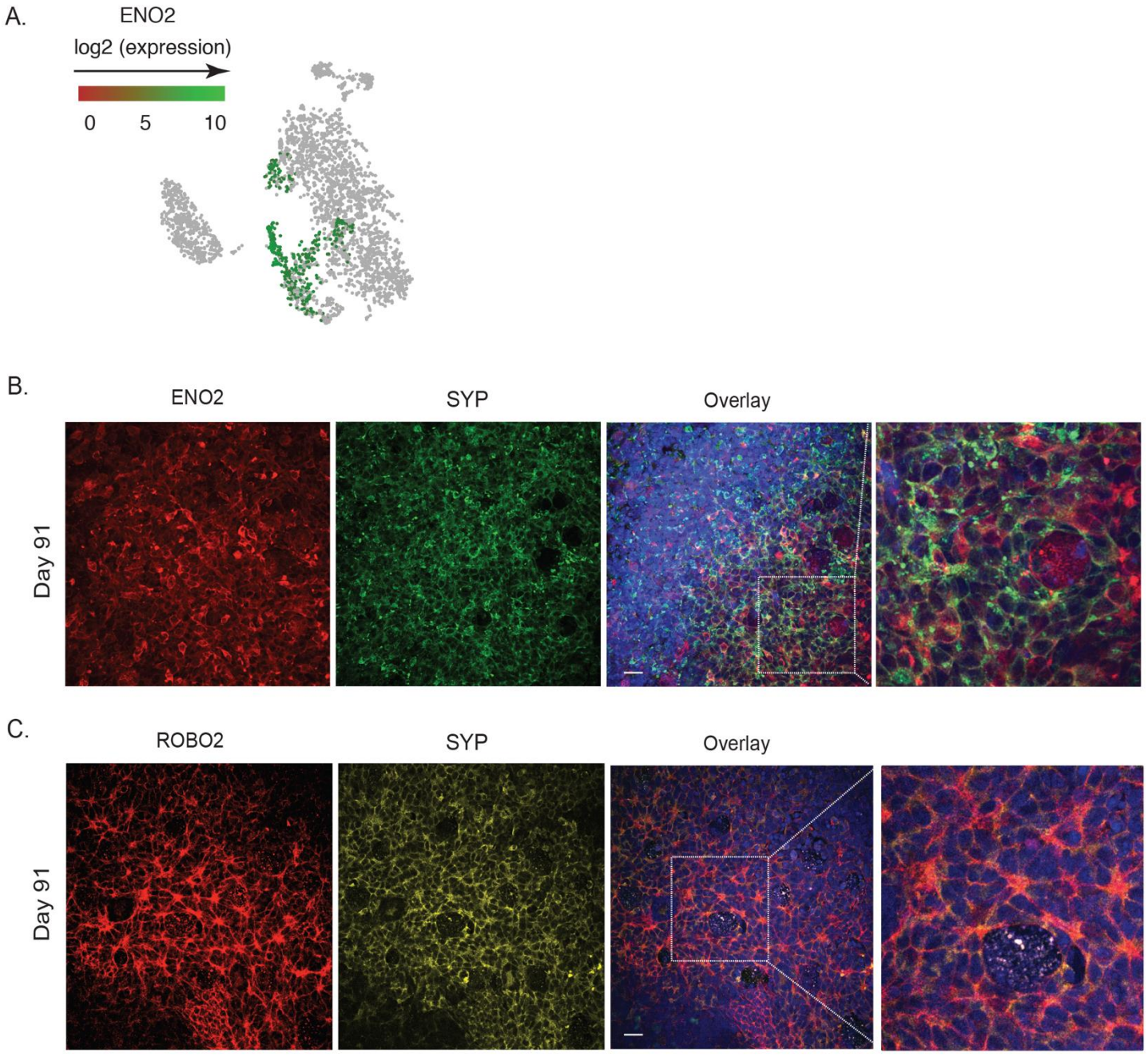
A.
ENO2
log2 (expression)
0
5
10
B.
ENO2
SYP
Overlay
Day 91
C.
ROBO2
SYP
Overlay
Day 91

Figure S6

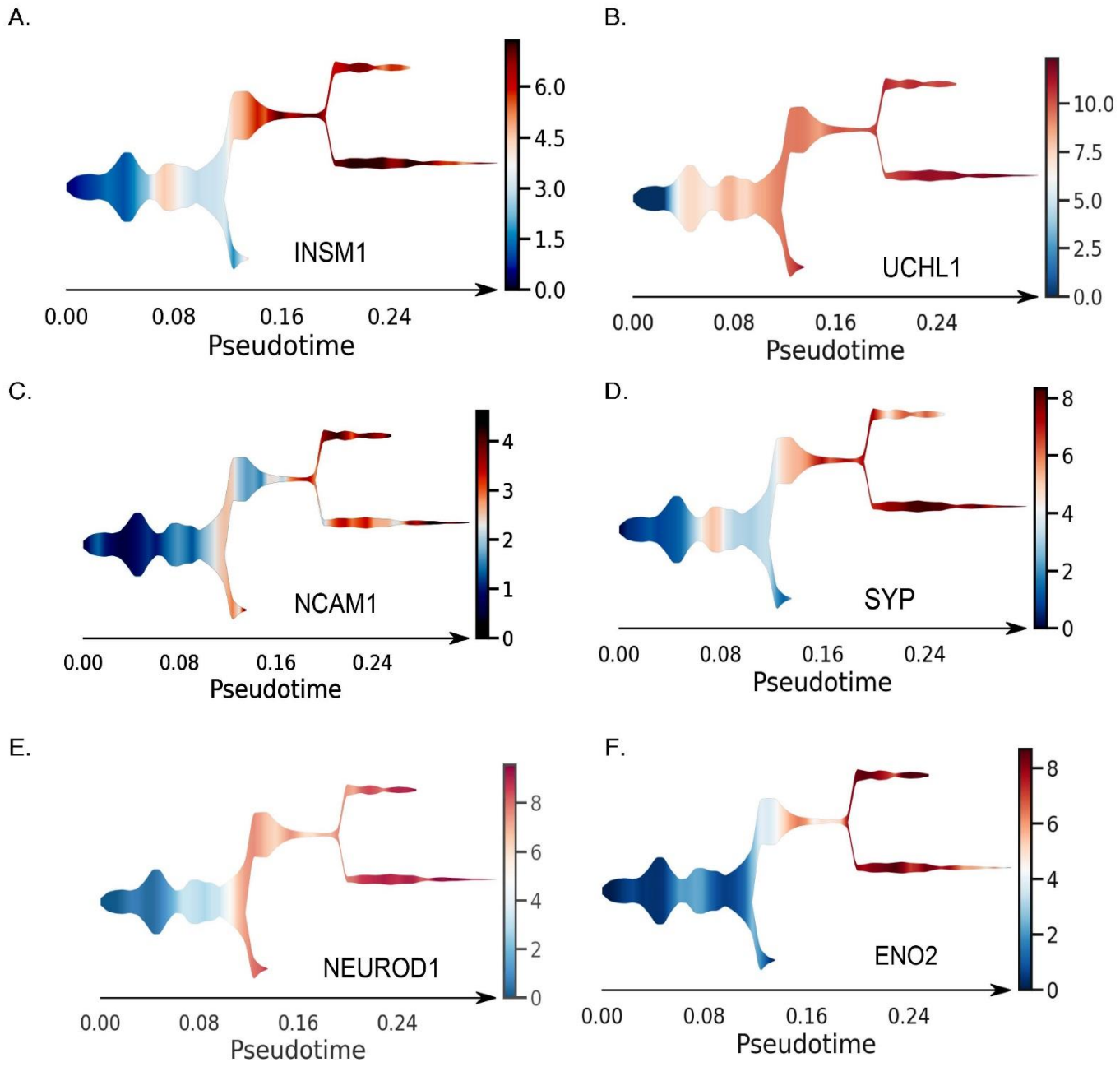
A.
INSM1
6.0
4.5
3.0
1.5
0.0
0.00
0.08
0.16
0.24
Pseudotime
B.
UCHL1
10.0
7.5
5.0
2.5
0.0
0.00
0.08
0.16
0.24
Pseudotime
C.
NCAM1
4
3
2
1
0
0.00
0.08
0.16
0.24
Pseudotime
D.
SYP
8
6
4
2
0
0.00
0.08
0.16
0.24
Pseudotime
E.
NEUROD1
8
6
4
2
0
0.00
0.08
0.16
0.24
Pseudotime
F.
ENO2
8
6
4
2
0
0.00
0.08
0.16
0.24
Pseudotime

Figure S7

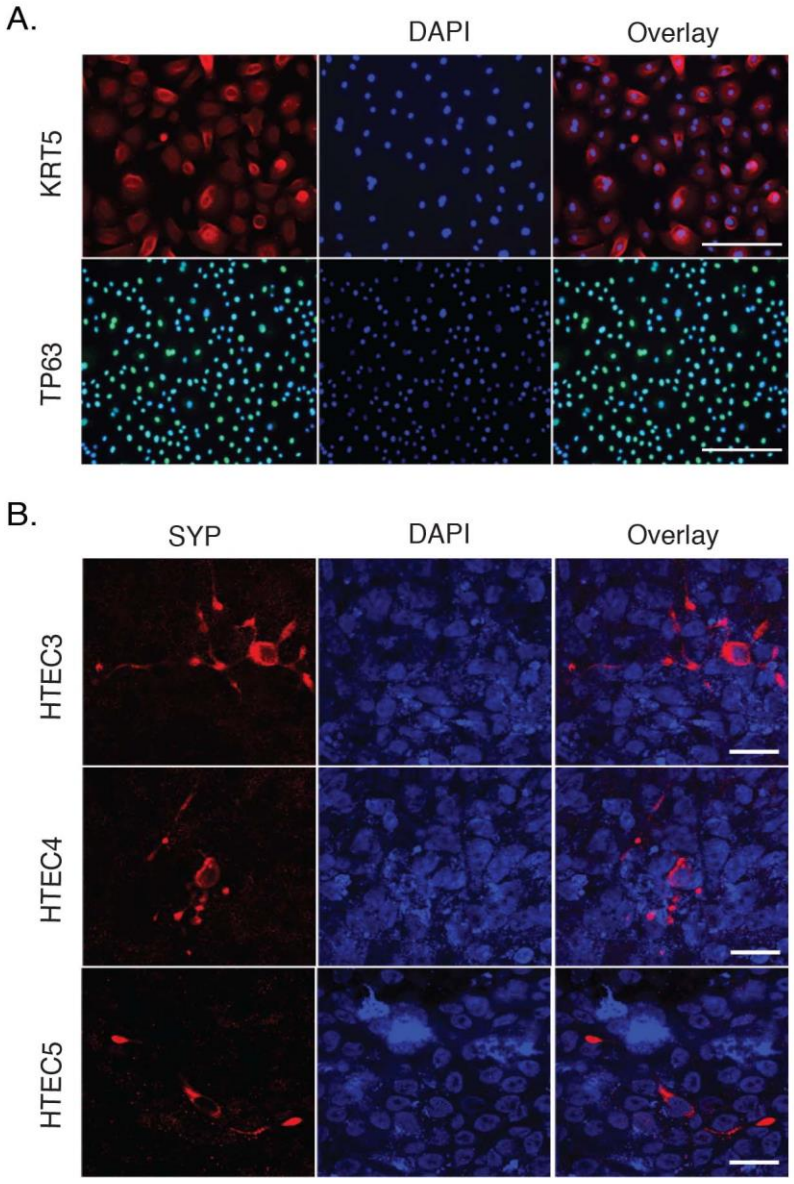
A.
DAPI
Overlay
KRT5
TP63
B.
SYP
DAPI
Overlay
HTEC3
HTEC4
HTEC5

Figure S8

Supplemental Tables:

Table S4. Primary antibodies related to Figures 1, 2, 3, 4 and Supplemental Figures S1, S2, S3, S4, S6 and S8.

Name	Brand	Catalog number	Dilutions
SYP	Abcam	ab32127	1:300
SYP	Santa Cruz Biotechnology	sc-17750: SYP (D-4)	1:100
ENO2	Santa Cruz Biotechnology	sc-271384: Enolase (A-5)	1:100
CHGA	Proteintech	60135-1-Ig	1:100
ROBO2	R&D Systems	AF3147	1:100
PGP9.5	Santa Cruz Biotechnology	sc-271639: UCH-L1 (C-4)	1:100
EPCAM	R&D Systems	AF960	1:100
VIM	Sigma-Aldrich	V6630	1:100
NKX2.1	Abcam	ab76013	1:100
KRT5	Biolegend	905901	1:100
TP63	Cell Signaling Technology	4892S	1:100

Table S5. Quantitative RT-PCR primers related to Figure 5 and Supplemental Figure S2.

Gene	Forward	Reverse
β-Actin	5'-CATGTACGTTGGTATCGAGGC-3'	5'-CTCCTTAATGTCACGCACGAT-3'
HES1	5'-ACGTGCGAGGGCGTTAATAC-3'	5'-GGGGTAGGTCATGGCATTGA-3'
HEY1	5'-AGAGTGCGGACGAGAATGGAAACT-3'	5'-CGTCGGCGCTTCTCAATTATTCCT-3'
ASCL1	5'-CCCAAGCAAGTCAAGCGACA-3'	5'-AAGCCGCTGAAGTTGAGCC-3'
GRP	5'-AAAGAGCACAGGGGAGTCTTC-3'	5'-TCCTTTGCTTCTATGAGACCCA-3'
DLL3	5'-CGTCCGTAGATTGGAATCGCC-3'	5'-TCCCGAGCGTAGATGGAAGG-3'
GAD67	5'-GCTTCCGGCTAAGAACGGT-3'	5'-TTGCGGACATAGTTGAGGAGT-3'
ENO2	5'-CTGATGCTGGAGTTGGATGG-3'	5'-CCATTGATCACGTTGAAGGC-3'
ROBO2	5'-GTTTGTGTTGCGAGGAACTATCT-3'	5'-GTTTTGTCGGAAGTCATCTCGTA-3'
SYP	5'-CTCAGCATCGAGGTCGAGTTC-3'	5'-GAGGAGTAGTCCCCAACTAAGAA-3'

Transparent Methods

iPSC reprogramming: Human fibroblasts were reprogrammed into iPSCs using lentiviral encoded human reprogramming factors (Oct4, Lin28, cMyc, Klf4, Sox2) along with an shRNA targeting human p53 (Firth et al., 2014). Briefly, 1x 10^5 cells were transduced with recombinant viral particles for 24-48 hours and plated on feeder cells. Twenty-four hours later the media was changed to iPSC media (KO DMEM, 20% KO serum replacement, 0.01mM β Mercaptoethanol, 1% NEAA, 1% Glutamax (all Invitrogen) and 10 ng/ml FGF-2) and subsequently replaced every other day. For titer calculation, 293T cells were transduced by different reprogramming viruses for 2 days and percent of transduced cells was determined by staining for OCT4. Colonies displaying good stem cell morphology were individually picked and expanded, usually around day 15-21. Two additional human lymphoblastoid cell lines from healthy subjects (ND00184 and ND03719) were obtained from the National Institute of Neurological Disorders and Stroke (NINDS) Biorepository at the Coriell Institute. These lines were reprogrammed into iPSCs and served as biological replicates (labeled 'iPSC1' and 'iPSC2' respectively in Fig. S1A). These lines were created using episomal plasmids, encoding 5 factors POU5F1, SOX2, KLF4, MYCL, and

LIN28A and an shRNA to p53 (Okita et al., 2013) and maintained on Geltrex (Life Technologies) or Matrigel (BD Bioscience) in mTeSR1 medium (STEMCELL Technologies) supplemented with penicillin/streptomycin.

Differentiation to airway epithelium: Transwell inserts were coated with a combination of fibronectin (5 µg/mL; BD Biosciences), laminin (5 µg/mL; Sigma-Aldrich), and collagen IV (60 µg/mL; Sigma-Aldrich), or six-well plates were coated with Geltrex at a 1:200 dilution from a 15 mg/ml stock (Thermo Fisher Scientific, A1413302). iPSCs were dissociated to a single-cell suspension using Accutase (Stemcell Technologies, 7920). Then, 300,000 iPSCs were plated per 30-mm insert or 120,000 per 12-mm insert in mTeSR (Stemcell Technologies, 85850) with 10 µM ROCK inhibitor Y-27632 (Selleckchem, Houston, TX, S1049) for 24 hours. iPSCs were then differentiated through definitive endoderm, anterior foregut endoderm and lung-specific endoderm stages (Firth et al., 2014). All media compositions used for the differentiation are the same as in the original protocol. For some experiments, small molecule γ-secretase inhibitors DAPT (Cayman Chemical, Ann Arbor, Michigan, 208255-80-5) or dibenzazepine (DBZ, Cayman Chemical, Ann Arbor, Michigan, 209984-56-5) were added at concentrations of 1, 10 and 20 µM (for DAPT) or 0.5, 2 and 5 µM (for DBZ), starting at Day 17 of differentiation until the experimental end point, with media changes every other day.

Immunocytochemistry: Cells were fixed in 3.2% (vol/vol) paraformaldehyde (PFA) for 1 hour at 4°C, washed 3X with phosphate-buffered saline (PBS), and permeabilized in 0.5% Triton X-100 for 1 hour at 4°C. Cells were blocked for 1 hour with commercial CAS block (Thermo Fisher Scientific, 008120) and then incubated in primary antibody (Supplemental Table S2) at 4°C overnight. Cells were washed 3X in 0.1% Triton X-100 in PBS and incubated for 1 hour in secondary antibodies. Stained cells were then incubated with DAPI for 5 min before washing and mounting on glass microscope slides in Immunomount (Thermo Fisher Scientific, 9990402). Alternately, cells were washed after secondary antibody incubation and directly mounted on the glass microscope slide using Vectashield with DAPI (Vector Laboratories, Burlingame, CA, H-1500). Images were captured at either 20X, 40X or 63X on a Zeiss LSM 800 confocal microscope at the USC Optical Imaging Facility (Los Angeles, CA) and processed/counted using Image J (Schneider et al., 2012).

Immunohistochemistry: Explanted human lung tissues were obtained in compliance with an Institutional Review Board approved protocol (HS-18-00273) for using human source material in research and the research was

considered exempt. Tissues were fixed for 24 hours in formalin, embedded in paraffin and sectioned at 10 µm thickness. Paraffin-embedded sections were deparaffinized by washing 3 x 4 min in 100% toluene, 1 x 3 min in 95% EtOH (vol/vol), 1x 3 min in 70% EtOH (vol/vol), 1 x 3 min in 50% EtOH (vol/vol) and finally with distilled water. Antigen retrieval buffer (Sigma) was pre-heated to 95°C, and slides were incubated for 30 min and allowed to cool for 20 min at room temperature. Slides were blocked in CAS block for a minimum of 1 hour before staining in primary antibody (Supplemental Table S2) overnight at 4°C. Sections were washed 3x in 0.1% Triton X-100 in PBS and incubated for 1 hour in secondary antibody. Slides were mounted using Vectashield with DAPI (Vector Laboratories). Images were captured at 20X, 40X or 63X on a Zeiss LSM 800 confocal microscope at the USC Optical Imaging Facility.

Quantitative RT-PCR: Total RNA was isolated using the Qiagen RNA Easy Mini Kit (74004, 74134) as per the manufacturer's protocol. Then, 500 ng of RNA was DNase-treated (Worthington Biochemical Corporation, Lakewood, NJ, LS003172) per the manufacturer's protocol and reverse-transcribed to cDNA using a Protoscript first strand synthesis kit (New England Biolabs, E6560S). Quantitative PCR was performed using SYBR Green (Biorad, 1725125) in a 5 µl reaction volume at 50 °C for 2 min, 95 °C for 10 min, 95 °C for 15 s, and 60 °C for 1 min for 40 cycles and analyzed using 7900HT SDS software (Biorad). Each run consisted of triplicate technical repeats per experiment. Beta-actin was used as an internal control. The data were normalized to Day 0 for Fig 3D to observe the overall increase/decrease in key PNEC marker expression over 90 days of differentiation. For Supplemental Fig S1D-G, the data were normalized to Day 5 in order to compare the expression of individual markers with an earlier time point during differentiation rather than starting iPSCs at Day 0. Since Day 0 iPSCs tend to have some expression of some of these markers it makes it harder to track smaller gene expression changes over first 30 days of differentiation. Data are expressed as normalized cycle threshold (Ct) ± SEM. Primers used for qRT-PCR are included in Supplemental Table S3.

Single cell RNA sequencing**:** Day 91 differentiation cultures were dissociated for 30 mins at 37^{o}C using Accutase to obtain single-cell suspensions. Cells were stained with DAPI and sorted for live single cells followed by cDNA library preparation per the Chromium Single-Cell 30 Library Kit (10x Genomics) manufacturer's guide at the Genomics Core of the Department of Biomedical Sciences at Cedars-Sinai Medical Center and sequenced using

the 10X Genomics platform on a Next Seq 500. Two experimental replicates of 2113 cells and 2039 cells were sequenced at 260-280 million reads per sample.

Single cell RNA-seq data analysis to identify iPNEC-associated genes**:** Raw reads from the 10X Genomics platform were de-multiplexed using barcode processing and then aligned to the human reference genome (GRCh 38) using STAR aligner. Mitochondrial genes and low abundance genes were filtered out. Post-normalization expression counts for each gene were collapsed and normalized to unique molecular identifiers (UMI) to generate an expression matrix. The count data were analyzed based on the methodology reported by Lun *et al*. (Lun et al., 2016). A total of 1705 and 1502 cells were selected respectively from each replicate post quality control filtering for further analysis. Based on the log transformed counts, a total of 1171 differentially expressed (DE) genes were identified to be common between both replicates within the iPNEC cluster in comparison to other clusters (Kolodziejczyk et al., 2015). All further analyses were done using this selection of 1171 DE genes. Graph-based clustering followed by statistical ANOVA test was used to identify biomarkers of each cluster. The clustered data was visualized using t-SNE and PCA plots. The PNEC clusters were identified by using a gene set enrichment analysis with various human tissues and cells as reference using the K- nearest neighbor algorithm (R-package Weighted k-Nearest Neighbors for Classification).

Pseudotemporal reconstruction of differentiation trajectories: Cell fate decisions and differentiation trajectories were reconstructed with the single-cell trajectories reconstruction, exploration and mapping v4.1 (H. Chen et al., 2019). It incorporates a Modified Local Linear Embedding (MLLE) along with ElPiGraph (Lever et al., 2016; Zhang and Wang, 2006) and is not dependent on the predefined number of branches thereby allowing an unbiased study of lineage potential across a heterogeneous population (Qiu et al., 2017). To define the developmental trajectories, we used cluster-based MST (minimum spanning tree) analysis to infer the lineage structure. We used normalized expression values to generate a pseudotime plot that can account for both branched and linear differentiation processes. We have further analyzed the potential marker genes associated with each trajectory and its branching. Additionally, we have used the Monocle package that uses reverse graph embedding to reconstruct lineage trajectories (Trapnell, 2020; Trapnell et al., 2014a, 2014b). We selected cells, that were projected onto specific lineages based on the branches termed as cell ‘‘states”. Subsequently, we

reran the Monocle3 algorithm and assigned basal cells as starting cell lineage until only a single/ simple trajectory was identified.

Enzyme-linked immunosorbent assay (ELISA): ELISA was performed using Human Enolase 2/Neuron-specific Enolase Quantikine ELISA Kit (R&D systems), as per the manufacturer's instructions. The experiment was repeated four times with basal media and iPSC-conditioned media as controls.

Differentiation of HTEC: Human donor lung specimens were dissected into smaller segments for dissociating and harvesting the airway cells (Gu et al., 2014). Total epithelial cell yield will vary depending upon tissue viability and size. Airway epithelial cells were seeded on to collagen IV-coated transwell membranes. A collagen stock (Corning, 3470) of 60 µg/mL was used as the working solution for coating membrane surfaces. The day after seeding the media was removed from the apical surface (air-interfacing) and from there on the cultures were maintained under air-liquid-interface (ALI) conditions. The experiment was repeated with HTEC preparations from seven different donor lungs.

Image analysis: Images captured on an LSM 800 confocal microscope were quantified and analyzed using ImageJ (Schneider et al., 2012).

iPNEC quantification: To quantify iPNECs in a given culture, the mean fluorescence intensity of the antibody stain and DAPI were quantified for 10-12 images (which covered almost the entire filter) at 20X magnification per time point/condition. For all quantifications, unless otherwise mentioned, percentage of MFI was calculated for each marker fluorescence relative to total DAPI fluorescence, followed by statistical analysis.

iPNEC branching analysis: To measure the phenotypic complexity of iPNECs, we used the Sholl analysis plugin on ImageJ, commonly used for analyzing neuronal arbors (https://imagej.net/Sholl_Analysis), to measure the extent of iPNEC intersections. 10-12 images at 20X magnification per time point/condition were used for the analysis of each marker. For Sholl analysis, the outputs measured were number of intersections (I) and branching

density (I/area of analyzed) (Binley et al., 2014; Bird and Cuntz, 2019; “Sholl Analysis,” n.d.; Sholl, 1953; Stanko and Fenton, 2017).

Statistical analysis: All experiments were conducted using at least three technical replicates (e.g., three 6-wells or Transwells) from the same differentiation. All experiments were performed (independent differentiations) at least three times except where otherwise indicated. Unless otherwise noted, all analyses were performed in GraphPad Prism v.6. All data are presented as mean ± SEM. Statistical significance was determined by Student’s t test (two-tailed) between two groups. Three or more groups were analyzed by one-way analysis of variance (ANOVA). $P < 0.05$ was considered statistically significant.

Accession numbers: Raw scRNAseq data of primary human fetal lung-derived PNECs have been deposited in the EMBL-EBI ArrayExpress database (Accession number: E-MTAB-8221).

Supplemental References

Binley, K.E., Ng, W.S., Tribble, J.R., Song, B., Morgan, J.E., 2014. Sholl analysis: A quantitative comparison of semi-automated methods. Journal of Neuroscience Methods 225, 65–70. https://doi.org/10.1016/j.jneumeth.2014.01.017

Bird, A.D., Cuntz, H., 2019. Dissecting sholl analysis into its functional components. Cell Rep 27, 3081-3096.e5. https://doi.org/10.1016/j.celrep.2019.04.097

Branchfield, K., Nantie, L., Verheyden, J.M., Sui, P., Wienhold, M.D., Sun, X., 2016. Pulmonary neuroendocrine cells function as airway sensors to control lung immune response. Science 351, 707–710. https://doi.org/10.1126/science.aad7969

Chen, H., Albergante, L., Hsu, J.Y., Lareau, C.A., Lo Bosco, G., Guan, J., Zhou, S., Gorban, A.N., Bauer, D.E., Aryee, M.J., Langenau, D.M., Zinovyev, A., Buenrostro, J.D., Yuan, G.-C., Pinello, L., 2019. Single-cell trajectories reconstruction, exploration and mapping of omics data with STREAM. Nat Commun 10, 1903. https://doi.org/10.1038/s41467-019-09670-4

Firth, A.L., Dargitz, C.T., Qualls, S.J., Menon, T., Wright, R., Singer, O., Gage, F.H., Khanna, A., Verma, I.M., 2014. Generation of multiciliated cells in functional airway epithelia from human induced pluripotent stem cells. Proc. Natl. Acad. Sci. U.S.A. 111, E1723-1730. https://doi.org/10.1073/pnas.1403470111

Gu, X., Karp, P.H., Brody, S.L., Pierce, R.A., Welsh, M.J., Holtzman, M.J., Ben-Shahar, Y., 2014. Chemosensory functions for pulmonary neuroendocrine cells. Am J Respir Cell Mol Biol 50, 637–646. https://doi.org/10.1165/rcmb.2013-0199OC

Kolodziejczyk, A.A., Kim, J.K., Tsang, J.C.H., Ilicic, T., Henriksson, J., Natarajan, K.N., Tuck, A.C., Gao, X., Bühler, M., Liu, P., Marioni, J.C., Teichmann, S.A., 2015. Single Cell RNA-Sequencing of pluripotent states unlocks modular transcriptional variation. Cell Stem Cell 17, 471–485. https://doi.org/10.1016/j.stem.2015.09.011

Lever, J., Krzywinski, M., Altman, N., 2017. Principal component analysis [WWW Document]. Nature Methods. https://doi.org/10.1038/nmeth.4346

Lever, J., Krzywinski, M., Altman, N.S., 2016. Points of Significance: Classification evaluation. Nat Methods 13, 603–604. https://doi.org/10.1038/nmeth.3945

Lun, A.T.L., Bach, K., Marioni, J.C., 2016. Pooling across cells to normalize single-cell RNA sequencing data with many zero counts. Genome Biol. 17, 75. https://doi.org/10.1186/s13059-016-0947-7

Okita, K., Yamakawa, T., Matsumura, Y., Sato, Y., Amano, N., Watanabe, A., Goshima, N., Yamanaka, S., 2013. An efficient nonviral method to generate integration-free human-induced pluripotent stem cells from cord blood and peripheral blood cells. Stem Cells 31, 458–466. https://doi.org/10.1002/stem.1293

Qiu, X., Mao, Q., Tang, Y., Wang, L., Chawla, R., Pliner, H.A., Trapnell, C., 2017. Reversed graph embedding resolves complex single-cell trajectories. Nat Methods 14, 979–982. https://doi.org/10.1038/nmeth.4402

Schneider, C.A., Rasband, W.S., Eliceiri, K.W., 2012. NIH Image to ImageJ: 25 years of image analysis. Nature Methods 9, 671–675. https://doi.org/10.1038/nmeth.2089

Sholl Analysis [WWW Document], n.d. . ImageJ. URL https://imagej.net/Sholl_Analysis (accessed 7.22.19).

Sholl, D.A., 1953. Dendritic organization in the neurons of the visual and motor cortices of the cat. J Anat 87, 387-406.1.

Stanko, J.P., Fenton, S.E., 2017. Quantifying branching density in rat mammary gland whole-mounts using the sholl analysis method. JoVE (Journal of Visualized Experiments) e55789. https://doi.org/10.3791/55789

Trapnell, C., 2020. monocle: Clustering, differential expression, and trajectory analysis for single- cell RNA-Seq. Bioconductor version: Release (3.10). https://doi.org/10.18129/B9.bioc.monocle

Trapnell, C., Cacchiarelli, D., Grimsby, J., Pokharel, P., Li, S., Morse, M., Lennon, N.J., Livak, K.J., Mikkelsen, T.S., Rinn, J.L., 2014a. The dynamics and regulators of cell fate decisions are revealed by pseudotemporal ordering of single cells. Nat. Biotechnol. 32, 381–386. https://doi.org/10.1038/nbt.2859

Trapnell, C., Cacchiarelli, D., Grimsby, J., Pokharel, P., Li, S., Morse, M., Lennon, N.J., Livak, K.J., Mikkelsen, T.S., Rinn, J.L., 2014b. Pseudo-temporal ordering of individual cells reveals dynamics and regulators of cell fate decisions. Nat Biotechnol 32, 381–386. https://doi.org/10.1038/nbt.2859

Zhang, Z., Wang, J., 2006. MLLE: Modified Locally Linear Embedding Using Multiple Weights, in: NIPS. https://doi.org/10.7551/mitpress/7503.003.0204